Duct effects on acoustic source radiation

Benjamin Baddour, * Phillip Joseph, † Alan McAlpine ‡ and Ronnie Leung §

This paper presents a detailed numerical investigation into the effects of a semi-infinite hard-walled duct on the radiation due to point dipole sources rotating around the duct axis. In particular, this paper is concerned with the effect of source position relative to the duct open end and its comparison with radiation in a free field. This study was motivated by the increasing tendency for ducted propellers and fans to be located close to the open end relative to the acoustic wavelength. In this study the conditions are established under which duct effects on source radiation may be neglected.

*Postgraduate Researcher, Institute of Sound and Vibration Research, University of Southampton, Southampton, SO17 1BJ UK, contact: bb2u19@soton.ac.uk

†Professor of Engineering Acoustics, Institute of Sound and Vibration Research, University of Southampton, Southampton, SO17 1BJ UK, contact: pfj.isvr@soton.ac.uk

‡Associate Professor, Institute of Sound and Vibration Research, University of Southampton, Southampton, SO17 1BJ UK, contact: am.isvr@soton.ac.uk

§Principal Engineer, Defence Science and Technology Laboratory, Fareham, PO17 6AD UK, contact R.E.leung@soton.ac.uk

Nomenclature

a	duct radius
A_{mn}	pressure amplitude
c_0	ambient speed of sound
D	polar directivity (non-dimensional)
F	magnitude of fluctuating force (dipole source strength)
k	acoustic wavenumber
k_z	axial wavenumber
N	total number of modes
p	acoustic pressure
t	observer time
t_0	emission time
W	acoustic power

Coordinates:

(R, ϕ, θ)	spherical polar coordinates
(r, θ, z)	cylindrical polar coordinates
(x, y, z)	Cartesian coordinates

Greek symbols:

η	free-field to ducted power ratio (non-dimensional)
κ	transverse wavenumber
ϕ_{mn}	mode-ray angle/ nil-shielding direction
ϕ_{los}	highest angle of clear line of sight
χ	accumulated phase angle (non-dimensional)
ω	angular frequency
Ω	Rotational speed

Subscripts:

0	source location
F	flanged
m	azimuthal order
n	radial order

Superscripts:

ff	free-field
D	Ducted

Other symbols:

$\tilde{}$	Transformed variable
$\bar{}$	Mean variable
$\hat{}$	Time domain variable

I Introduction

Many propeller and rotor systems are ducted to enhance their efficiency and to improve safety, such as aero-engine rotors and marine propellers. The prediction of the acoustic radiation due to ducted rotors and propellers typically requires analysis of the behaviour of the individual duct modes excited by the rotor so that their contribution to the far-field can be predicted. However, this detailed analysis can be avoided if the difference between the far-field radiation from free-field and ducted sources is known *a priori*, assuming that the source distribution is unaffected by the duct. Moreover, analysis of this difference provides fundamental insight into the effect of the duct on rotor and propeller radiation.

Surrounding a fan, propeller or rotor has two effects. The first is to modify the flow around the fan, which of course alters the source strength of sound. The second modifies the radiation, which is subject of this paper in which we study the difference between ducted and free field, in the absence of flow. The industrial application for this work is therefore ducted marine propellers, where the flow Mach number is negligible and industrial cooling fans.

One application where this approximation is not valid is of course in aero-engine turbofan engine applications, where the flow influences the transmission and sound radiation from the fan. This application would of course require the full solution to the Euler or Navier Stokes equations and is outside the scope of this paper. Nevertheless, even in this case, quantifying the effect by the duct on source radiation independently of the source is useful.

To the authors' knowledge the only study aimed at comparing the radiation due to free-field and ducted sources was by Chapman [1]. Chapman investigated in detail the behaviour of the open-to-ducted transfer function for a single azimuthal acoustic mode. One of the important aspects of his study was the identification of 'nil-shielding' angles at which the radiation from the free-field and ducted sources is identical. The existence of nil shielding directions was demonstrated analytically from the solutions of the radiation directivity of single acoustic modes from a flanged duct.

Chapman's comparison of free-field and ducted radiation [1] is confined to a single propagating azimuthal mode order m and does not address the differences for arbitrary source distributions, which can potentially excite all possible acoustic modes, including cut-off modes. This paper is a study of the comparison of the acoustic radiation due to point dipole sources with arbitrary orientation rotating around an axis either within a semi-infinite, hard-walled circular duct or located in a free-field.

The analysis coordinate system for the free-field and ducted cases are presented in Figs 1a and 1b respectively. In both cases a point force with arbitrary time dependence (magnitude $F(t)$) is assumed to rotate at angular velocity Ω around the z axis with radius of rotation r_0. The point force is assumed to be orientated at angle γ between the azimuthal and axial dimensions. Far-field observer points are expressed in a spherical coordinate system at position (R, ϕ, θ) centred on a point located at an axial distance z_0 from the centre of rotation $(x, y, z) = (0, 0, 0)$, where R is the radial distance and θ and ϕ are the azimuthal and polar angles respectively. The azimuthal position is in the θ-direction measured anticlockwise from the x-axis, and the polar coordinate is in the ϕ-direction measured from the z-axis. In figure 1b the rotating dipole source is assumed to be located within a semi-infinite, hard-walled, un-flanged circular duct of radius a.

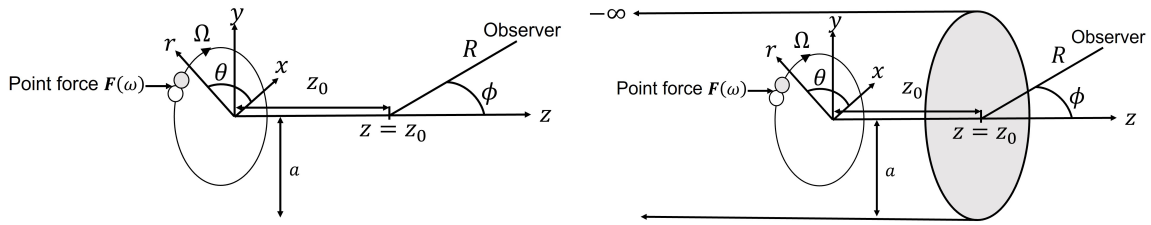

(a) Free-field source **(b) Ducted source**

Figure 1 Coordinate system of free-field and ducted sources

I.A Radiation from free-field point rotating dipole sources

In this section the solution for the free-field radiation due to rotating point dipole sources is reviewed. This problem has been addressed by a number of authors for a steady force, for example Garrick and Watkins [2], Hanson [3], Parry and Crighton [4], Schulten [5], Peake and Crighton [6], Mao, Gu, Qi and Tang [7], McAlpine and Kingan [8] and Blake [9]. The essential difference between these various studies is the choice of coordinate system, hence these may be shown to provide consistent solutions when expressed in a common coordinate system [1].

In Appendix A, the solution of the acoustic radiation due to a rotating point dipole with arbitrary time dependence is derived. The frequency domain solution $\tilde{p}^{(ff)}(R, \phi, \theta, \omega)$, is shown in the Appendix to be in the form of a summation of azimuthal acoustic mode orders m,

$$\tilde{p}^{(ff)}(R, \phi, \theta, \omega) = \sum_{m=-\infty}^{\infty} \tilde{p}_m^{(ff)}(R, \phi, \theta, \omega) \, . \tag{1}$$

Each modal pressure contribution is of the form,

$$\tilde{p}_m^{(ff)}(R,\phi,\theta,\omega) = j^{m-1}\frac{1}{4\pi R}\left(\frac{m}{r_0}\sin\gamma + k\cos\phi\cos\gamma\right)\tilde{F}(\omega - m\Omega)J_m(kr_0\sin\phi)\mathrm{e}^{-jk(R-z_0\cos\phi)-jm(\theta-\overline{\theta_0})}, \tag{2}$$

where k is the acoustic wavenumber $k = \omega/c_0$ and c_0 is the sound speed, $\overline{\theta_0}$ and z_0 are the source azimuthal coordinate and distance between the source and the duct open end at emission time $t_0 = 0$ respectively. Note that the only effect on the solution due to source rotation is the introduction of a Doppler shift on the source frequency $\tilde{F}(\omega - m\Omega)$.

I.B Acoustic radiation from a semi-infinite duct

In this section the solution for the far-field radiation due to the point dipole source shown in figure 1b is reviewed. The source can be observed to rotate around its axis located within a semi-infinite, hard-walled, un-flanged circular duct.

The general solution for the far-field radiation when the source is located within the duct is now in the form of a summation of azimuthal and radial mode orders with indices m and n,

$$p^{(D)}(R,\phi,\theta,\omega) = \sum_{m=-\infty}^{\infty}\sum_{n=1}^{\infty} p_{mn}^{(D)}(R,\phi,\theta,\omega)\,, \tag{3}$$

with each modal contribution of the form,

$$p_{mn}^{(D)}(R,\phi,\theta,\omega) = \left(\frac{a}{R}\right)A_{mn}(\omega - m\Omega)D_{mn}(\phi,ka)\,\mathrm{e}^{-j(kR+m\theta)}\,, \tag{4}$$

where $A_{mn}(\omega - m\Omega)$ is the complex modal pressure amplitude, and $D_{mn}(\phi, ka)$ is the non-dimensional far-field polar modal directivity function.

For the rotating point dipole force $A_{mn}(\omega - m\Omega)$ is derived in Appendix B, and is of the form,

$$A_{mn}(\omega-m\Omega) = \frac{1}{2S}\left[\frac{a}{r_0}m\sin\gamma + k_{z,mn}a\cos\gamma\right]F(\omega-m\Omega)\frac{1}{k_{z,mn}a\sqrt{1-\frac{m^2}{(\kappa_{mn}a)^2}}}\frac{J_m(\kappa_{mn}r_0)}{J_m(\kappa_{mn}a)}\mathrm{e}^{j(k_{z,mn}z_0+m\tilde{\theta}_0)}, \tag{5}$$

where $S = \pi a^2$ is the area of the duct cross-section, $k_{z,mn}$ is the modal axial wavenumber, and κ_{mn} is the transverse wavenumber chosen to satisfy the hard-walled boundary condition, $\partial p/\partial r = 0$ at $r = a$. The wavenumbers are

related through the dispersion relationship,

$$k^2 = \kappa_{mn}^2 + k_{z,mn}^2. \tag{6}$$

The solution for the directivity function $D_{mn}(\phi, ka)$ for both flanged and un-flanged ducts are discussed in the next section.

I.C Far-field modal directivity functions for ducted sources

The modal radiation due to ducted sources has been addressed by a number of authors. The first work on the far-field radiation due to a single acoustic mode incident upon the open end of a flanged duct was by Tyler and Sofrin [10] in 1962.

Subsequently, Homicz and Lordi [11] developed an expression for the far-field modal pressure from a semi-infinite, hard-walled, un-flanged circular duct using the Wiener-Hopf technique. Their solution does not readily allow computation of the radiation due to cut-off modes, $\kappa_{mn} < k$, and is therefore unsuitable for calculations where the source is located relatively close to the duct open end, $z_0/\lambda \to 0$. More recently Gabard and Astley [12] provided an alternative formulation that readily includes cut-off modes (and also the effect of flow and a center-body both of which will not be considered in the present study).

The flanged solution has been shown to provide a good approximation to the un-flanged result for polar angles not too close to the sideline directions $\phi \approx 90°$ and for modes not too close to the cut-off frequency ($k/\kappa_{mn} = 1$).

All predictions comparing free-field and ducted directivities presented in this paper have been calculated using the un-flanged solution, specifically the solution by Gabard and Astley [12], who expressed the modal directivity function for a hard-walled hollow duct in the form,

$$D_{mn}(\phi, ka) = \frac{(ka + k_{z,mn}a)(1 - \cos\phi)}{\pi(k_{z,mn}a - ka\cos\phi)ka\sin\phi H_m'(ka\sin\phi)\sqrt{(1 - \frac{m^2}{\kappa_{mn}^2 a^2})}} \frac{K_m^-(\kappa_{mn}a)}{K_m^+(\cos\phi)}\,. \tag{7}$$

In Eq. 7 H_m is the Hankel function of the first kind with prime denoting differentiation with respect to its argument, and K^+ and K^- are the Kernel functions, which are determined from complex integral expressions.

By contrast, the solution for the modal radiation from a flanged duct derived by Tyler and Sofrin [10], $D_{F,mn}(\phi, ka)$,

is considerably simpler and provides much greater insight into the behaviour and characteristics of modal radiation from ducts. It is of the form

$$D_{F,mn}(\phi, ka) = j^{m-1}\frac{k_{z,mn}}{k}\frac{\sin\phi J'_m(ka\sin\phi)}{(\frac{\kappa_{mn}^2}{k^2} - \sin^2\phi)\sqrt{(1-\frac{m^2}{\kappa_{mn}^2 a^2})}}\,. \tag{8}$$

Comparisons between the flanged and un-flanged directivities for modes excited above and below cut-off are shown in figure 2 for a mode of azimuthal order $m = 9$ and radial order $n = 6$. Results are shown at three different frequencies representing cut-off ratios of $k/\kappa_{mn} = 1.5, 1.01$ and 0.5, corresponding to a well cut-on mode, a mode just cut-on, and a mode well cut-off respectively.

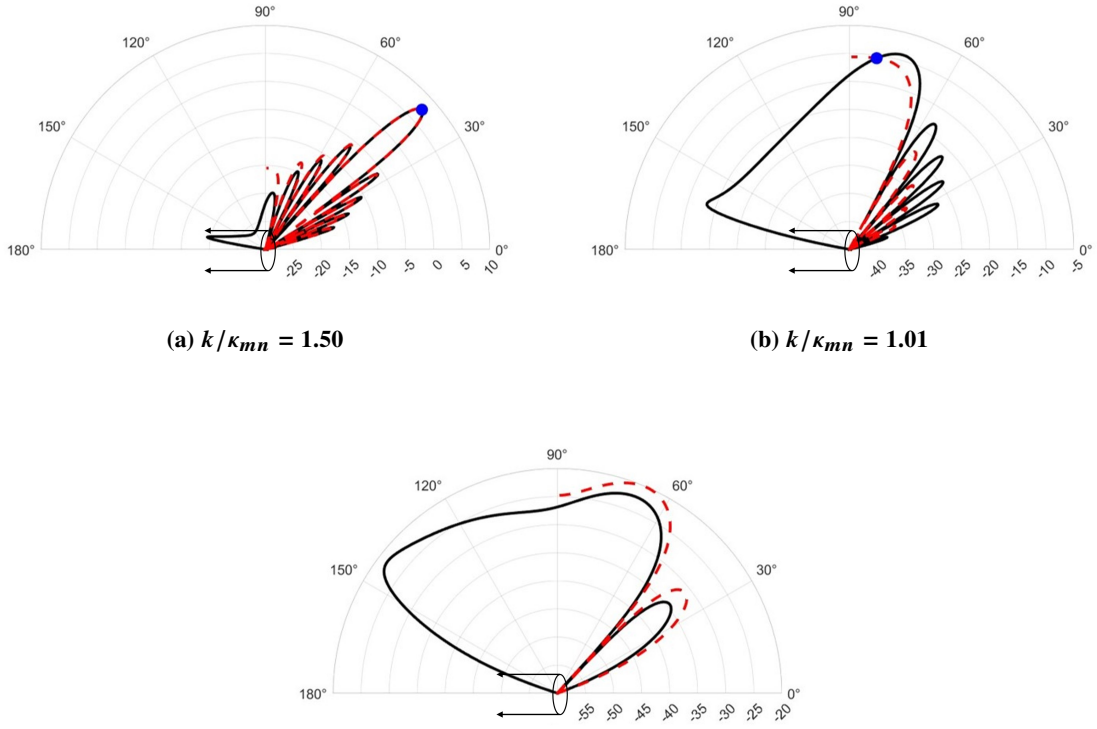

(a) $k/\kappa_{mn} = 1.50$ **(b) $k/\kappa_{mn} = 1.01$**

(c) $k/\kappa_{mn} = 0.50$

Figure 2 Modal directivity for $(m, n) = (9, 6)$ at $k/\kappa_{mn} = 1.5, 1.01$ and 0.5. The un-flanged directivity - solid black line, flanged - red dashed line, mode-ray angle Eq. 9 -blue circle. In *dB* re 1.

Whilst the general shape of the directivity functions presented in figure 2 are similar in the forward arc, their levels can be observed to be significantly different by up to 5 *dB* in these examples. However, despite these

large differences, the two solutions $D_{mn}(\phi, ka)$ and $D_{F,mn}(\phi, ka)$ are in very close agreement at the angles ϕ_{mn}, given by

$$\sin \phi_{mn} = \frac{\kappa_{mn}}{k}. \tag{9}$$

These angles have been identified by a number of authors as the mode-ray angle at which peak radiation occurs for well cut-on modes, as in figure 2a. However, Chapman [1] showed that these angles have broader significance as the 'nil-shielding' angles at which the free-field and ducted solutions agree, but without providing examples. The existence of nil-shielding directions is shown in this paper to be central to the understanding between the differences in the characteristics of the radiation from free-field and ducted sources.

Note when the mode is cut-off, as shown in figure 2c, the angle ϕ_{mn} is not defined. For the remainder of this paper we use the directivity function of Gabard and Astley [12] to predict the radiation from roating point dipole sources, considering modes excited above and below cut-off.

II Nil-shielding directions

Following Chapman [1] the existence of nil-shielding directions is readily demonstrated for the flanged duct by evaluating $p_{F,mn}(R, \phi, \theta, \omega)$ (substituting Eq. 8 into Eq. 4) at the nil-shielding direction $\phi = \phi_{mn}$ by the use of L'Hôpital's rule to give,

$$p^{(D)}_{F,mn}(R, \phi_{mn}, \theta, \omega) = j^{m-1} \left(\frac{1}{4\pi R}\right) \left[\frac{m}{r_0} \sin\gamma + k \cos\phi_{mn} \cos\gamma\right] F(\omega - m\Omega) J_m(kr_0 \sin\phi_{mn}) \mathrm{e}^{-jk(R - z_0 \cos\phi_{mn}) - jm(\theta - \tilde{\theta}_0)}. \tag{10}$$

This expression is identical to Eq. 2 derived in Appendix A for the far-field pressure due to the same source radiating into a free-field, thereby demonstrating that at these mode-ray angles, the rigid duct is effectively transparent to sound, where radiation from the duct is equal to the free-field source. We further note by observation of figure 2 that the un-flanged duct solution is also in agreement with the free-field and flanged duct solutions. It therefore follows that the flanged duct, un-flanged duct, and free-field solutions are in agreement in the forward arc at the mode-ray nil-shielding directions, i.e.

$$p^{(D)}_{mn}(R, \phi_{mn}, \theta, \omega) = p^{(ff)}_{m}(R, \phi_{mn}, \theta, \omega). \tag{11}$$

Chapman [1] stated that this behaviour was 'strikingly evident' from the predictions for free-field and ducted source radiation in Myers and Lan [13]. Attempts at proving the agreement between the expression for $p_m^{(ff)}(R, \phi_{mn}, \theta, \omega)$ and $p_m^{(D)}(R, \phi_{mn}, \theta, \omega)$ at $\phi = \phi_{mn}$ involving the un-flanged directivity expression of Eq. 7 have so far been unsuccessful owing to the complexity of the Kernel function K.

II.A Far-field directivities for single azimuthal modes due to sources deep inside the duct

The previous section has investigated the characteristics of the far-field radiation for single acoustic duct modes and verified the existence of nil-shielding directions, which occur at the mode-ray angles, where the solution is in exact agreement with the free-field solution.

Before comparing the directivities due to ducted and free-field sources for calculations involving multiple azimuthal mode orders, directivities for some idealised cases involving only a single azimuthal mode order are compared to highlight more clearly the role of nil-shielding directions in determining the overall directivity in the forward arc.

The directivities between free-field and ducted sources are now investigated for a single azimuthal mode order m when the source plane is $z_0/\lambda = 5$, which, acoustically, is far from the duct open end such that the contribution due to cut-off modes can be neglected. Figures 3a and 3b show a comparison between the free-field and ducted directivities for the single azimuthal mode order $m = 0$, excited at $ka = 5$ and 35 respectively. The radius of rotation and dipole orientation are chosen to be $r_0/a = 0.5$ and $\gamma = 0°$ respectively. The fluctuating force strength spectrum is taken to be 'flat' with unit source strength $\tilde{F} = 1$. Throughout this paper, the expression for the far-field is evaluated at $R = 1\,m$. The nil-shielding directions for each constituent radial mode order n are represented by the blue circles.

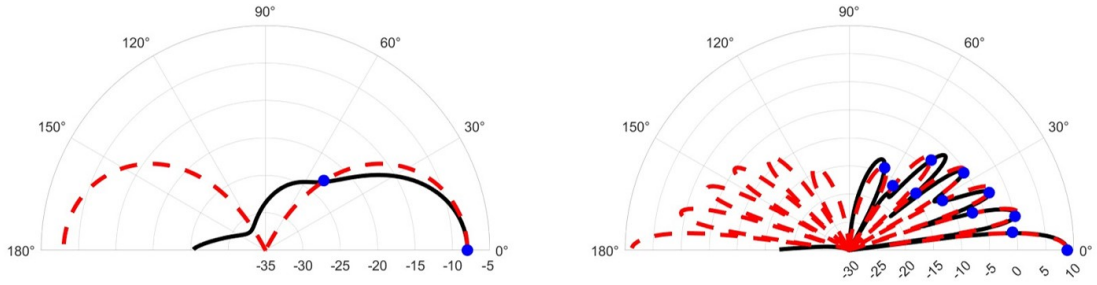

(a) $ka = 5$ **(b)** $ka = 35$

Figure 3 Free-field (red dashed line) and ducted (black line) directivities of rotating point dipole sources for $m = 0$, with $r_0/a = 0.5$, $z_0/\lambda = 5$ and $\gamma = 0°$, with nil-shielding directions as the blue circles. In *dB* re 1 *Pa*

The important feature of figure 3 is that, even when multiple radial mode orders are present, very close agreement is observed between the un-flanged ducted solution and the free-field solution at the nil-shielding directions ϕ_{mn}. At $ka = 35$ there are eleven cut-on modes for $m = 0$, whereas at $ka = 5$ there are only two. Clearly, therefore, the presence of additional radial modes do not disrupt the agreement between the two solutions at the nil-shielding directions. This property was recognised by Chapman [1] for the flanged-duct directivity, which he attributed to the 'interlacing' property of the Bessel function appearing in the expression for $D_{mn}(\phi)$. In terms of the directivity function, this property may be stated as,

$$\begin{aligned} D_{mn'}(\phi_{mn}, ka) &= 0, \qquad && n \neq n', \quad \forall k \\ D_{mn'}(\phi_{mn}, ka) &\neq 0, && n = n', \quad k < \kappa_{mn} \end{aligned} \tag{12}$$

In figure 3a for $ka = 5$ and $m = 0$, only the plane wave mode $(m, n) = (0, 1)$ and mode $(m, n) = (0, 2)$ are cut-on, and hence only two nil-shielding directions occur at which the solutions can be observed to exactly match, with the plane wave having $\phi_{mn} = 0°$. Deviations between the solutions of up to 3 *dB* can be observed at angles away from the nil-shielding directions (in the majority of the forward-arc). At the much higher non-dimensional frequency of $ka = 35$, many more radial modes and hence nil-shielding directions are present at which the solutions match. Due to the high density of nil-shielding directions at this frequency good agreement between the two solutions occur, not only at the nil-shielding directions, but also at angles in-between. Naturally there is no agreement in the rear-arc $90° < \phi < 180°$ which is shielded by the duct unlike for a free-field source, which is exactly symmetric about $\phi = 90°$ in this example with $\gamma = 0°$ (axial dipole).

II.B Far-field directivities for single azimuthal modes due to sources at the open end

As the source plane approaches the duct open end the contribution from cut-off modes become increasingly important to the overall far-field radiation. To illustrate the importance of the location of the source plane to overall radiation for the single azimuthal mode orders $m = 0, 1, 2$ and 3, and hence to the contribution from cut-off modes, figures 4a - 4d shows the far-field directivity when the source plane is now located approximately at the duct open end. Also shown in the figure is the corresponding free-field directivity. In this example, $z_0/\lambda = 0.01$ and $ka = 5$. In each figure the directivity due to the ducted radiation is further broken down into their contribution from cut-on modes and cut-off modes as the blue and grey lines respectively. Note the number of cut-off modes was chosen to ensure convergence of the directivity function. which is typically many times the number of cut-on modes. The remaining parameters as the same as in figure 3a.

Note that Eq. 4 for the ducted radiation tends to infinity when the source is located exactly at $z_0/\lambda = 0$, as was shown in Baddour et al [14]. This behaviour was attributed to the number of cut-off modes that contribute significantly to the far-field radiation, which tends to infinity as the source approaches the duct open end. The reason for this behaviour in the formulation is still not resolved and is under further investigation. This was also noted by Rienstra and Tester [15], where they identified a divergent behavior of adding cut-off modes to compute the in-duct pressure field.

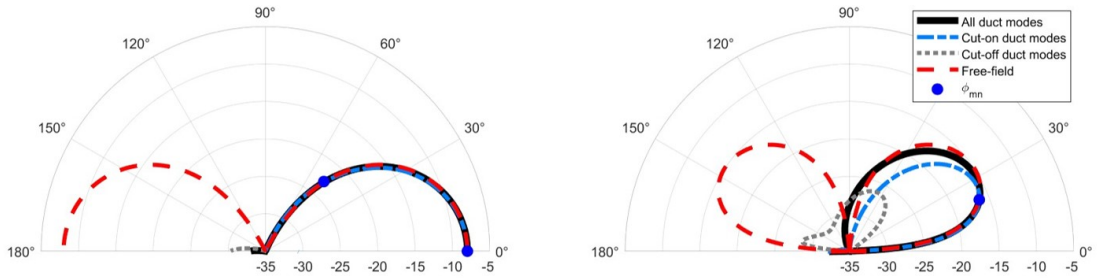

(a) $m = 0$ **(b)** $m = 1$

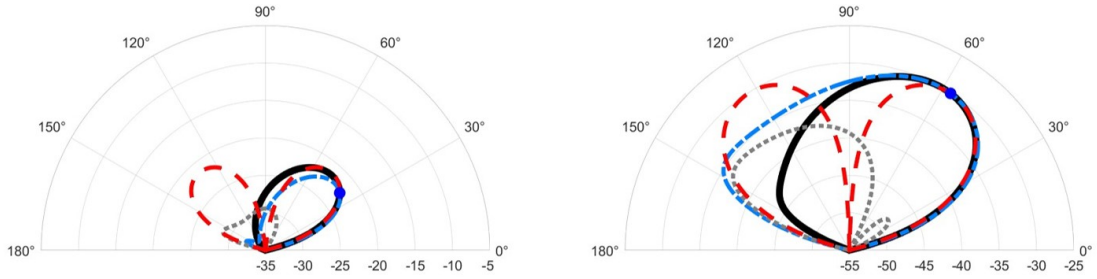

(c) $m = 2$ **(d)** $m = 3$

Figure 4 Free-field (red dashed line) and ducted (black line) directivities of rotating point dipole sources for $m = 0, 1, 2$ and 3 at $ka = 5$ with $r_0/a = 0.5$, $z_0/\lambda = 0.01$ and $\gamma = 0°$, with nil-shielding directions as the blue circles. In *dB* re 1 *Pa*. In *dB* re 1 *Pa*

For the zero mode order $m = 0$, only two radial modes are cut-on at this frequency whose nil-shielding directions can be seen at exactly 0° and approximately 50°. Excellent agreement is obtained between the ducted and free-field solutions, not only at these nil-shielding angles, but also at all angles in the forward arc. Note that in this case there is negligible contribution from cut-off modes. For mode order $m = 1$, however, excellent agreement is limited to angles less than the first nil-shielding direction of $\phi_{mn} \approx 20°$. Note that over this range of angles the contribution from cut-on modes is dominant. At angles greater than $\phi \approx 20°$ the agreement between the free-field and ducted solution is less good but remains within 2 *dB* at all angles up to $\phi \approx 120°$, which can be seen to be attributed to the presence of cut-off modes. For mode orders $m = 2$ and $m = 3$, good levels of agreement (< 1 *dB*) is observed at all angles up to approximately the first nil-shielding direction of $\phi_{mn} \approx 37°$ and $\phi_{mn} \approx 57°$ respectively, although the level of agreement can be seen to degrade with increasing m. At the higher angles, generally poor levels of agreement between the free-field and ducted solutions are observed. The contribution from cut-off modes becomes progressively weaker since their radiation efficiency has been shown to vary as $(ka)^{2m+2}$ [16]. In summary, therefore, generally good agreement is observed between the ducted and free-field directivities in all cases at radiation angles close to the duct axis but worsens significantly towards the sideline directions.

By contrast, significant deviations between the free-field and ducted directivities were observed in figure 3a at the comparatively low frequency of $ka = 5$ when the source plane was many wavelengths ($z_0/\lambda = 5$) from the duct open end, except at the nil-shielding directions where exact agreement was observed.

The reason for the difference in levels of agreement for the two source planes can be attributed to the phase

difference between different radial modes at the duct open end. Equation 2 for the free-field radiation includes the phase term $e^{jkz_0\cos\phi}$, while for ducted sources the far-field pressure contains the phase term $e^{jk_{z,mn}z_0}$ (see Eq. 5). Clearly therefore, the phase difference between the various radial mode orders at the duct open end are only equal:

1) At the nil-shielding directions $\phi = \phi_{mn}$.
2) At all radiation angles ϕ when the source plane is located at the duct open end $z_0 = 0$.

This is an important result which suggests that, for a single azimuthal mode order, the far-field radiation due to free-field and ducted sources is identical at the nil-shielding directions and becomes almost identical over a large range of forward arc angles as the source plane is moved increasingly closer to the duct open end. Clearly therefore, when the source is at the open end, the duct has a relatively small effect on the radiation of the source in the forward arc.

The comparison between free-field and ducted source directivities presented above (for an axial location $z_0/\lambda = 0.01$) is now shown at the much higher frequency of $ka = 35$, for azimuthal mode orders $m = 0, 10, 20$ and 30, in figure 5a - 5d respectively. The parameters are the same as in figure 3b.

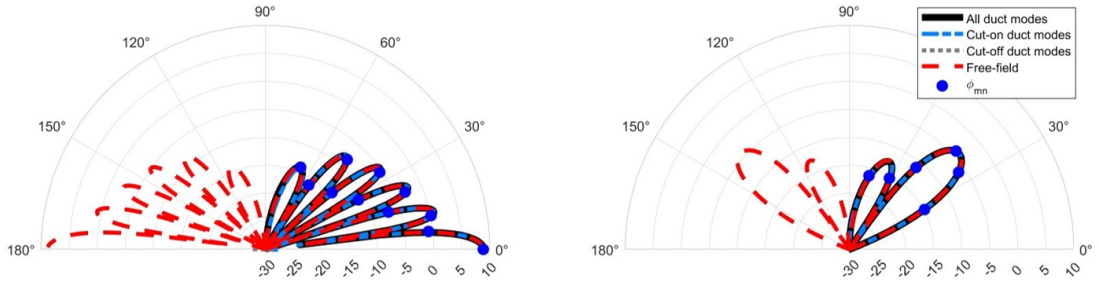

(a) $m = 0$ **(b)** $m = 10$

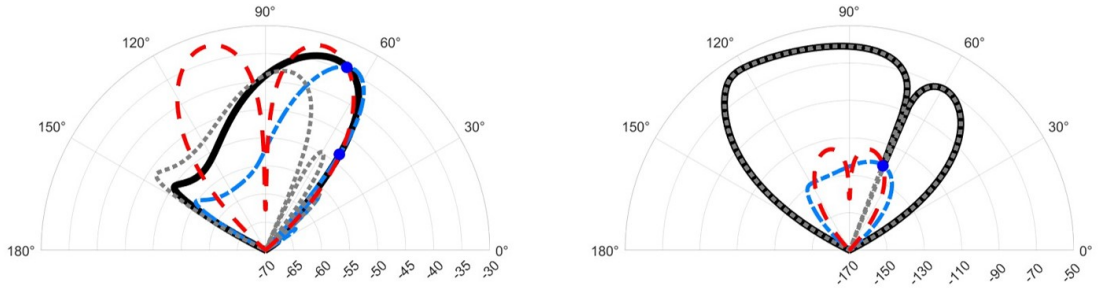

(c) $m = 20$ **(d)** $m = 30$

Figure 5 Comparison between free-field and ducted directivities of rotating point dipole sources at single azimuthal orders $m = 0, 10, 20$ and 30 at non-dimensional frequency $ka = 35$. Shown for a source radius of rotation $r_0/a = 0.5$, dipole orientation $\gamma = 0°$ and axial location $z_0/\lambda = 0.01$. The contribution of cut-on and cut-off modes are highlighted for the ducted case and the nil-shielding directions are shown as the blue circles. In *dB* re 1 *Pa*

By comparison with the previous results at $ka = 5$, in figure 5 the free-field and ducted solutions at this higher frequency are now in excellent agreement over a much larger range of angles for the azimuthal orders $m = 0, 10$ and 20. This improved level of agreement is due to the much higher number of nil-shielding directions present for $m = 0, 10$ and 20. At $m = 0$ and $m = 10$, contributions from cut-off modes can be observed to be negligible. However, at $m = 20$ the directivity levels can be observed to be significantly weaker than at the lower orders by about 10 to 20 dB, and hence the relative contribution from cut-off modes is more significant. For this mode the directivity is dominated by the cut-on modes at angles up to the second nil-shielding direction at $\phi_{mn} \approx 65°$, but then becomes dominated by the cut-off modes at higher angles.

At the highest azimuthal mode order under investigation, $m = 30$, the overall directivity is many orders of magnitude smaller than for the lower orders by virtue of its intrinsically weaker radiation efficiency. The notable aspect of the directivity for this azimuthal mode is that cut-off modes completely dominate the overall response (gray curve hidden below the black curve) except at the single nil -shielding direction at $\phi_{mn} \approx 68°$. Here, the contribution due to cut-off modes exhibits a null and the free-field and ducted solutions still agree.

Note that there exists a lower-bound frequency below which no nil-shielding directions can occur at which all radial mode orders associated with the same azimuthal mode order are cut-off. An estimate for these frequencies is readily obtained by noting that the first stationary value of the Bessel function of order m, $J'_m(\kappa_{m0}a) = 1$ occurs approximately at $\kappa_{m0}a \approx m$. The lower boundary frequency f (in Hertz) for the azimuthal mode m below which

no nil-shielding directions occur is therefore given by $f < mc_0/2\pi a$.

II.B.1 High-*ka* limit, $ka \to \infty$

Following from the observations above, now consider the limiting behaviour of ducted source radiation in the high frequency limit, $ka \to \infty$. Irrespective of the source location relative to the duct open end, z_0, the existence of nil-shielding directions at the discrete mode-ray angles ϕ_{mn} is highlighted. In the high-ka limit, the mode-ray angles associated with a particular value of m tend towards a continuum of values and the expression for the far-field radiation due to a ducted source must therefore tend to that of the free-field source for almost *all* radiation angles in the forward-arc independent of its position relative to the duct open end. The radiation angles in the side-line directions however, will have a lower ducted than free-field radiation caused by reflections of the modes closest to cut-off.

II.C Summary

By way of summary, for sources located close to the duct open end the radiation due to a single azimuthal mode m and its comparison with free-field radiation can be summarised as follows:

1) The radiation is sensitive to source position relative to the duct open end at low frequencies where there are comparatively few nil-shielding directions. The sensitivity of the radiation to source position becomes much weaker as frequency is increased since there are a greater number of nil-shielding directions at which the ducted directivity matches the free-field solution.
2) For sources close to the duct open end there is close agreement between the free-field and ducted radiation at polar angles from 0° (the duct axis) up to the highest nil-shielding direction associated with the least cut-on propagating mode.
3) For sources close to the duct open end, far-field radiation appears to be dominated by cut-on modes, with relatively small contribution due to cut-off modes over the range of angles specified above in 2.
4) Cut-off modes are generally important to the overall directivity for the higher order azimuthal modes m ($1/2ka \lesssim m \lesssim ka$) at radiation angles above the highest nil-shielding direction $\phi > \phi_{mn}$, including in the rear-arc. The contribution of cut-off modes appear to improve the agreement between the free-field and ducted radiation at the higher angles above the highest nil-shielding directions.

III Comparison between the free-field and ducted directivities for rotating point dipole sources

The previous sections have compared the directivity patterns due to single azimuthal mode orders excited by free-field and ducted rotating sources. In this section the directivities are compared, now with all possible azimuthal mode orders, including cut-off modes for the case of the ducted source, included. This comparison is made for different axial distances from the duct open end z_0, source radii of rotation r_0, dipole orientations γ and non-dimensional frequencies ka.

The expression for the mean squared pressure due to free-field and ducted sources, with all possible azimuthal modes included, may be obtained by evaluating $\overline{p^2} = \frac{1}{2} E\{pp^*\}$, where p is the expression for either the free-field or ducted pressure given by Eq. 2 or Eq. 5 respectively, and $E\{\cdot\}$ denotes the expectation operator. This procedure results in the cross-spectral term $E\{F(\omega - m\Omega)F^*(\omega - m'\Omega)\}$. In this paper frequency incoherence is assumed in the source cross-spectrum, i.e. $E\{F(\omega - m\Omega)F^*(\omega - m'\Omega)\} = \overline{F^2}(\omega - m\Omega)\delta_{mm'}$, in Eqs. 2 and 5, where $\delta_{mm'}$ is the Knonecker delta function, i.e., that the source spectrum at different frequencies is incoherent. The final results are presented for the two solutions in the form,

$$\overline{p^2}^{(ff)}(R,\phi,\omega) = \frac{1}{2}\left(\frac{1}{4\pi R}\right)^2 \sum_{m=-\infty}^{\infty} \left(\frac{m}{r_0}\sin\gamma + k\cos\phi\cos\gamma\right)^2 \overline{F^2}(\omega - m\Omega) J_m^2(kr_0\sin\phi). \tag{13}$$

$$\overline{p^2}^{(D)}(R,\phi,\omega) = \frac{1}{2}\left(\frac{1}{4\pi R}\right)^2 \sum_{m=-\infty}^{\infty} E\left\{\left|\sum_{n=1}^{\infty} A_{mn}(\omega - m\Omega) D_{mn}(\phi, ka)\right|^2\right\}. \tag{14}$$

The assumption made above concerning the source frequency spectrum implies that the mean square pressure due to different azimuthal modes may be summed incoherently, while the radial modes within each azimuthal mode must be summed coherently. Note also that for more complex spatial source distributions, such as might be expected for fan noise, each radial mode order n is also likely to be incoherent, as verified experimentally by Castres et al [17].

Equation 13 may be developed further. Expanding the term $(m/r_0\sin\gamma + k\cos\phi\cos\gamma)^2$ and assuming a 'flat' source spectrum $\overline{F^2}(\omega) = \overline{F^2}$ (i.e. independent of frequency), Eq. 13 may be simplified by noting the following Bessel function identities:

$$\sum_{m=-\infty}^{\infty} J_m^2(\Theta) = 1 \quad (a), \qquad \sum_{m=-\infty}^{\infty} m J_m^2(\Theta) = 0 \quad (b), \qquad \sum_{m=-\infty}^{\infty} m^2 J_m^2(\Theta) = \frac{1}{2}\Theta^2 \quad (c), \tag{15}$$

which upon substitution into Eq. 13 gives,

$$\overline{p^2}^{(ff)}(R,\phi,\omega) = \frac{1}{2}\overline{F^2}\left(\frac{k^2}{4\pi R}\right)^2 \left(\frac{1}{2}\sin^2\gamma\sin^2\phi + \cos^2\phi\cos^2\gamma\right) . \tag{16}$$

Equation 15a is a standard result, while Eq. 15b arises since $mJ_m^2(\Theta)$ is an odd function in m. The authors cannot seem to find a reference to Equation 15c, which has only been proven numerically (although not shown here). The final result of Eq. 16 is particularly simple. It reduces to standard results for the axial and transverse dipole orientations of $\gamma = 0$ and $\gamma = 90°$. Note that Eq. 16 is independent of the radius of rotation r_0.

The free-field directivity for the rotating source is fundamentally different from that when the source is stationary. The far-field directivity for a stationary dipole is proportional to $\cos^2(\phi - \gamma)$, and therefore rotates with the dipole orientation γ such that maximum and zero radiation occurs at $\phi_{\max} = \gamma$ and $\phi_{\min} = \gamma + 90°$ respectively. For rotating dipole sources, however, the far-field directivity becomes modified by the effects of rotation according to $(1/2\sin\gamma\sin\phi + \cos\gamma\cos\phi)^2$.

III.A Effect of far-field radiation due to source axial distance from the duct open end

In section II it is established that for a single azimuthal mode order in the high-frequency limit, $ka \to \infty$, there is close agreement between the free-field and ducted directivities at all polar angles in the forward-arc, irrespective of the source location within the duct. Also observed is the good match between free-field and ducted source radiation at *all* frequencies with the source located at the duct open end. Since the contributions from individual azimuthal mode orders may be summed incoherently, it therefore follows that the same conditions apply to ensure close agreement between the free-field and ducted solutions for the case when all azimuthal mode orders are excited due to an arbitrary source distribution.

To confirm this hypothesis the effect of z_0 on far-field radiation in the multi-mode case is investigated by interrogating Eqs. 16 and 14. Figure 6 shows a comparison between the multi-mode free-field directivity patterns $\overline{p^2}^{(ff)}(R,\phi,\omega)$ and the ducted directivity patterns $\overline{p^2}^{(D)}(R,\phi,\omega)$ computed at the two axial locations of $z_0/\lambda = 5$ and $z_0/\lambda = 0.01$. In these simulations r_0, γ and R are identical to those in Section II, with unit source strength assumed, $\overline{F^2}(\omega - m\Omega) = 1$.

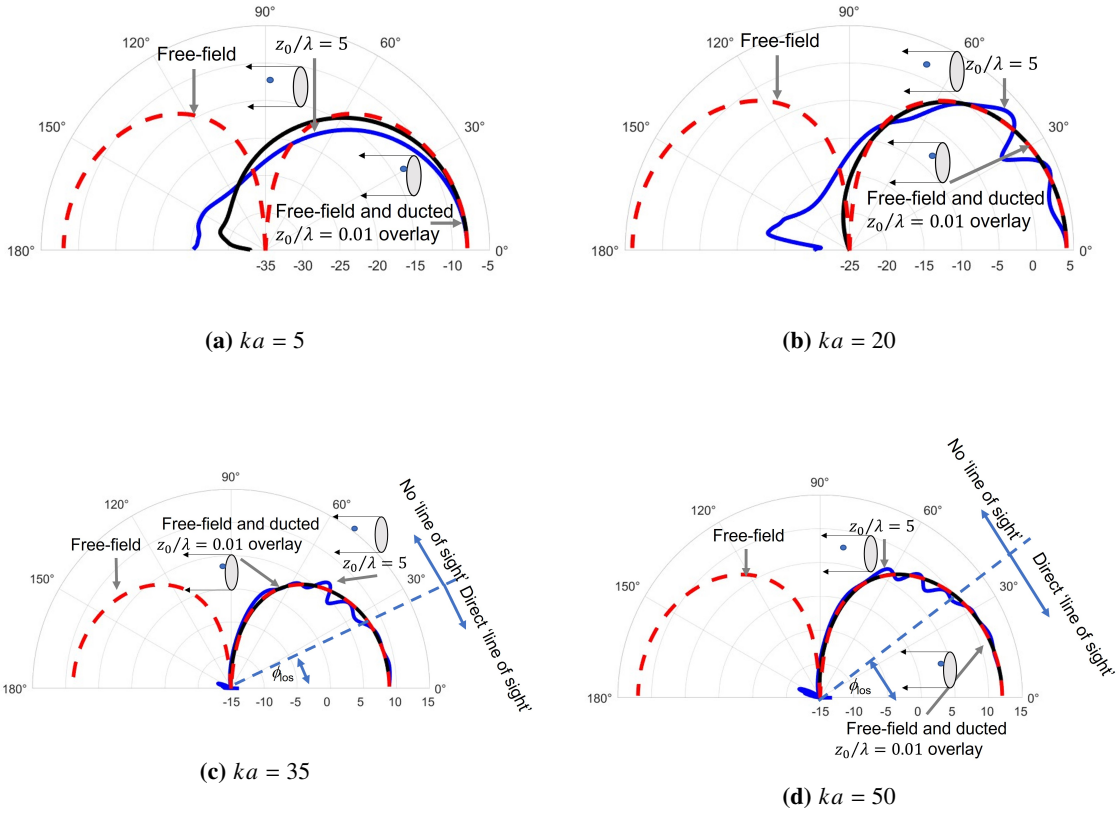

(a) $ka = 5$

(b) $ka = 20$

(c) $ka = 35$

(d) $ka = 50$

Figure 6 Free-field and ducted directivities of rotating point dipole sources with $r_0/a = 0.5$ and $\gamma = 0°$ at $ka = 5$, 20, 35 and 50, and$z_0/\lambda = 0.01$, $z_0/\lambda = 5$. In dB re 1 Pa.

Figure 6 shows that when the source plane is located at the duct open end, the free-field and ducted directivities generally agree to within 1 dB over a wide range of forward-arc angles at all frequencies. This result is consistent with the behaviour for single azimuthal modes m explored in Section II.

The most striking effect of locating the source deep within the duct $z_0/\lambda = 5$ is the appearance of oscillations in the far-field radiation, which in section II has been found to be caused by interference between different radial mode orders at the same azimuthal order. As frequency is increased the number of oscillations increase and becomes smaller in amplitude such that the ducted radiation tends to that of the free-field source. Although not seen in figure 6 for the axial dipoles, deviations from free-field behaviour is observed for non-axial dipoles where the radiation at $\phi = 90°$ is non-zero due to significant reflections of near cut-off modes.

III.B Effect of far-field radiation due to source radial position

This section investigates the effect on the far-field radiation due to source radius r_0/a from a rotating point dipole source. The same two axial locations investigated previously are used, $z_0/\lambda = 5$, where the effect of cut-off modes is negligible, and $z_0/\lambda = 0.01$, where cut-off modes make most contribution. Figures 7a - 7d show a comparison between the free-field and ducted directivities at the relatively low frequency of $ka = 5$ for an axial dipole source ($\gamma = 0°$). In each figure, results are shown for the two source radii of $r_0/a = 0$ and 1, which only affects the ducted radiation and not the free-field solution of Eq. 16. which in this case reduces to $\overline{p^2}^{(ff)} = \overline{F^2}\left(k^2/4\pi R\right)^2 \cos^2\phi \cos^2\gamma$. The remaining parameters are the same as in figure 6.

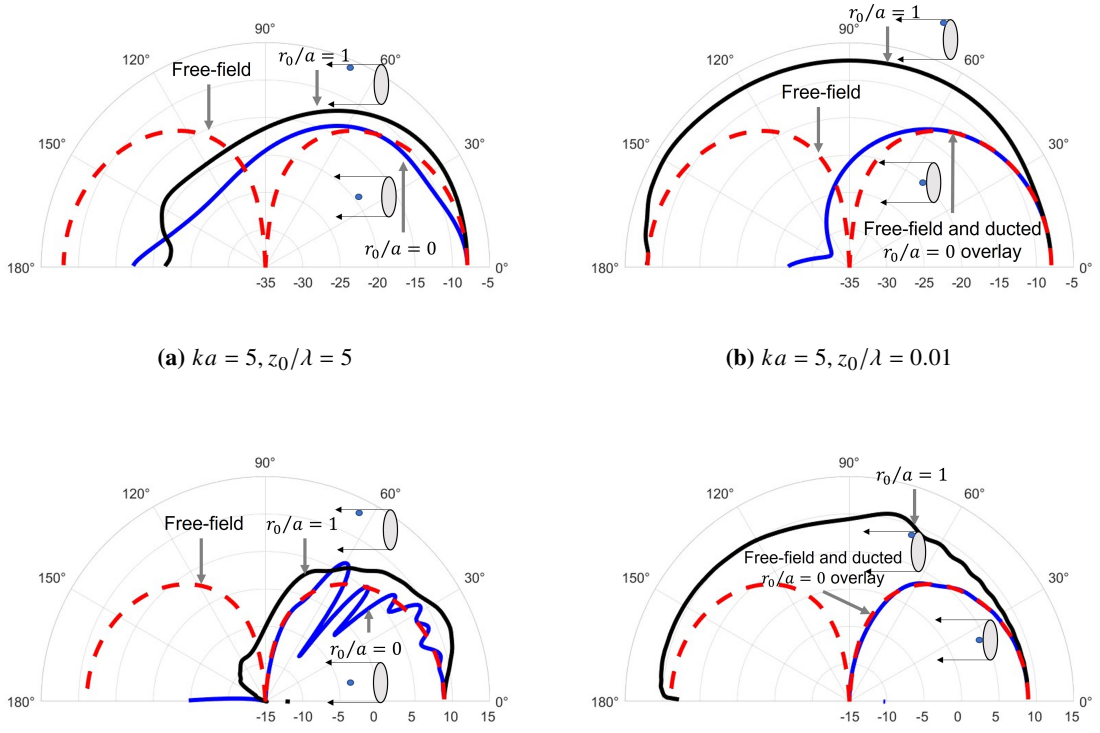

(a) $ka = 5, z_0/\lambda = 5$ **(b)** $ka = 5, z_0/\lambda = 0.01$

(c) $ka = 35, z_0/\lambda = 5$ **(d)** $ka = 35, z_0/\lambda = 0.01$

Figure 7 Free-field and ducted directivities of rotating point dipole sources with $r_0/a = 0.0$ and 1, $\gamma = 0°$. In *dB* re 1 *Pa*.

Figure 7 illustrates clearly the influence of both the source radius r_0 and axial location z_0 on the far-field directivity due to ducted sources. At the lowest frequency of interest, $ka = 5$, there is significant difference in level between the two ducted and free-field solutions when the source is deep within the duct. Note that when the source is located at the duct wall $r_0/a = 1$ the ducted radiation is approximately 3 *dB* greater than the free-field solution

over most of the range of angles. This finding is a result of the effective increase in acoustic pressure due to a source located next to a hard boundary. When the source is located on axis, far-field levels of radiation are observed to be similar.

However, when the source is located close to the duct open end, figure 7b and 7d indicates that the far-field directivity varies between that of a free-field axial dipole source when the source is on-axis $r_0/a = 0$, to being close to omni-directional when the source is located at the duct wall $r_0/a = 1$. Further investigations, shown in Section V.A below, indicated that this monopole-type behaviour only occurs when the source is a very small fraction of a wavelength close to the duct wall. Clearly, this difference between the dipole behaviour of figure 7a and the behaviour observed in figure 7b, which more closely resembles monopole type directivity is due to the significant contribution of the cut-off modes which are now important when the source is close to the duct open end. The clear conclusion is that locating the dipole source at the edge of a diffracting half-plane fundamentally alters the radiation to be similar to a monopole. The current mechanism for this behaviour is currently being explored.

Very similar behaviour to figures 7a and 7b can be observed in 7c and 7d at the much higher frequency of $ka = 35$. When the source is deep within the duct, evidence of strong interference between radial modes can be observed, which are absent when the source is located close to the duct open duct, as discussed previously in section III.A. Very close agreement is observed between the free-field and ducted sources when the source is on the duct axis, $r_0/a = 0$, but differs significantly when the source is on the duct rim, $r_0/a = 1$, and then radiates as a monopole.

Insight into the cause of the omni-directional behaviour for a source located at the duct rim observed in figure 7b and 7d can be obtained by splitting this directivity into contributions due to cut-on and cut-off modes, as shown in figure 8.

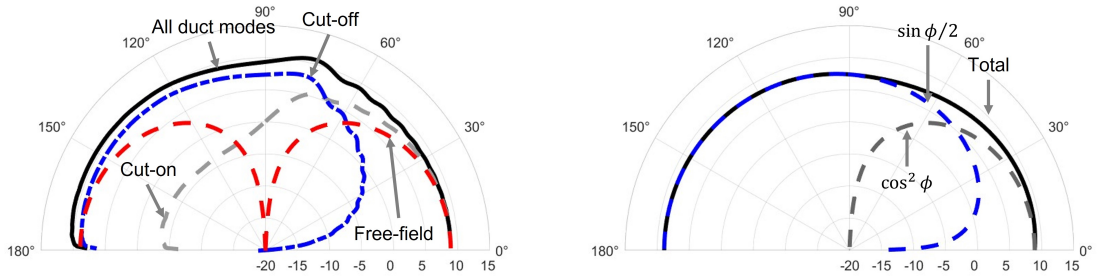

(a) Exact **(b) Theoretical**

Figure 8 Free-field and ducted directivities for rotating axial dipole sources with $r_0/a = 1$, $z_0/\lambda = 0.01$ at $ka = 35$, highlighting the contribution of cut-on and cut-off modes. In dB re 1 Pa.

Figure 8 demonstrates that the forward arc is dominated by propagating modes as observed previously. However, for the axial dipole source at the duct rim, cut-off modes become dominant in the rear-arc. An intriguing finding is that the radiation at $\phi = 0$ due to cut-on modes is equal to that at $\phi = \pi$ due to cut-off modes. When the pressure directivities from cut-on and cut-off modes are summed the resultant directivity is strongly omni-directional, as observed in the figure.

The forward-arc pressure closely follows the free-field directivity which is approximately $\cos\phi$. The rear-arc directivity can be observed to closely follow $\sin\phi/2$, as previously noted by Baddour et al [14], which is characteristic of the radiation directivity at distance R due to edge scattering of the form $R^{-1/2}\sin\phi/2$, which is the solution to Laplace's equation for incompressible flow due to a sharp edge, see Ffowcs Williams and Hawkings [18]. The resultant directivity is therefore the incoherent sum of the forward and rear-arc directivities, i.e.,

$$\overline{p^2}^{(D)}(R,\phi,\omega) \approx \begin{cases} \cos^2\phi + \sin\phi/2 & 0 < \phi < \pi/2 \\ \sin\phi/2 & \pi/2 < \phi < \pi, \end{cases} \tag{17}$$

These approximations are plotted in figure 8b with the level chosen to match the exact solution. Agreement between fig's 8a and 8b can be observed to be within about 1 dB at all radiation angles.

III.C Effect of far-field radiation due to dipole orientation

Finally, for completeness, this section presents an investigation of the effects of dipole orientation on the acoustic radiation from free-field and ducted sources. Figure 9 shows the free-field and ducted directivities, computed for $z_0/\lambda = 0.01$ at $ka = 5$ and 35, for the two dipole orientations of $\gamma = 45°$ and 90°. The remaining parameters are the same as in figure 6.

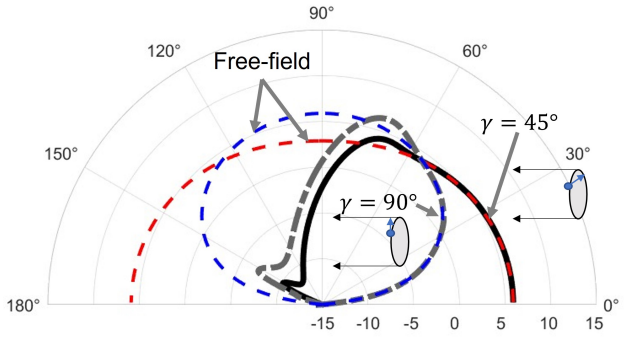

(a) $ka = 35$

Figure 9 Free-field and ducted directivities for rotating dipole sources at $ka = 35$ with $r_0/a = 0.5$, $z_0/\lambda = 0.01$ and $\gamma = 45°$ and 90°. In dB re 1 Pa.

Increasing the dipole orientation γ is shown to cause the main pressure lobe to approximately rotate towards the sideline directions, with the maximum radiation occurring at 90° for the transverse dipole $\gamma = 90°$. The level of agreement between the free-field and ducted sources is approximately the same as for the axial dipole source shown in figure 6c, suggesting that dipole orientation has no significant effect on the difference between free-field and ducted radiation.

IV Physical interpretation

Figure 6 has indicated that the agreement between the free-field and ducted directivities tend to converge over all forward-arc angles as the source is moved closer to the duct open end. However, for sources well away from the duct open end, good agreement with the free-field solution is confined to a range of shallow angles up to some particular polar angle but then begins to deviate at angles above this.

Two interpretations of these results are now discussed. The first is a ray interpretation, valid in the high frequency

$ka \to \infty$ limit. The second is based on a modal interpretation of the far-field radiation.

IV.A Ray theory interpretation

Simple physical reasoning can help to explain the reason why, for sources well away from the duct open end, close agreement between the free-field and ducted directivity patterns begins to deviate above some particular angle but agrees at all angles when the source is brought close to the duct open end, as observed in figs 6c and 6d. Invoking a ray interpretation of the solution in the high-frequency limit suggests that the effect of the duct on the source radiation is negligible at all radiation angles for which there is a clear 'line of sight' between the source and the far-field observer. By simple geometry, for a point source at radial position r_0 and distance z_0 from the open end a clear line of sight exists at all polar angles up to some maximum angle ϕ_{los} given by,

$$\phi_{los} = \tan^{-1}(a - r_0)/z_0. \tag{18}$$

For the cases under investigation with source axial location $z_0/\lambda = 5$, in figure 6c, ϕ_{los} corresponds to approximately 29°, and for figure 6d, it is approximately 39°. These range of angles are indicated in figure 6 and can be clearly seen to delineate the range of angles of good agreement and those where deviations begin to occur owing to duct diffraction effects.

As the non-dimensional frequency ka is increased, the influence on the forward-arc radiation due to the duct becomes increasingly weaker. This interpretation explains why the free-field and ducted solutions always agree on axis 0°. Note also that 0° represents the nil-shielding direction for the plane wave mode and this is the only mode that radiates at this angle.

However, as the source is moved deeper within the duct, the region of direct 'line of sight' reduces and the diffraction of the modes radiation owing to the duct starts to become significant.

IV.B Modal interpretation

The previous section developed a ray theory interpretation to explain the results shown in Figure 6. This section proposes an alternative interpretation based solely on the behaviour of individual duct modes. We now assume that the contribution to the forward arc pressure due to cut-off modes can be neglected, which is realistic for sources well away from the duct open end.

A single mode propagating within the duct towards the open end at some axial location z from the source plane is of the form $\mathrm{e}^{-jk_{z,mn}z}$. From the dispersion relation (Eq. 6) and the relationship between κ_{mn} and the nil-shielding direction ϕ_{mn} (Eq. 9), modal propagation within the duct can be written as $p_{mn} \propto \mathrm{e}^{-jk\cos\phi_{mn}z}$. The phase χ_{mn} accumulated by the mode in propagating a unit axial distance $z = 1$ along the duct is therefore,

$$\chi_{mn} = k\cos\phi_{mn} \ . \tag{19}$$

It is clear therefore that modes with nil-shielding directions close to the duct axis $\phi_{mn} \approx 0$, due to well cut-on modes, accumulate greatest phase χ_{mn}. Of interest here is the phase *difference* between modes with similar nil-shielding directions ϕ_{mn}. The phase difference $\delta\chi$ between any two modes with nil-shielding directions separated by $\delta\phi_{mn}$ is therefore approximately given by,

$$\delta\chi \approx -k\sin\phi\,\delta\phi_{mn} \tag{20}$$

A number of modes with nil-shielding directions close to the duct axis therefore arrive at the duct open end with relatively small phase difference compared to cut-on modes with nil-shielding directions close to $\phi \approx 90°$. This property is the cause of the oscillations observed in figure 6 at high radiation angles.

Equation 20 suggests that the modes responsible for the radiation close to the duct axis arrive with relatively small phase difference $\delta\chi$ and therefore radiate approximately in phase. At high radiation angles, however, oscillations appear in the ducted directivity due to phase interference between the modes responsible for the radiation at these high angles.

The degree of phase difference between the modes at the duct open end may be quantified by the use of Eq. 20 to compute the phase difference $\delta\chi$ between successive modes with nil-shielding direction separated by $\delta\phi$. This phase difference is plotted in figure 10 against ϕ_{mn} for the case considered in figure 6c where $z_0/\lambda = 5$ and $ka = 35$.

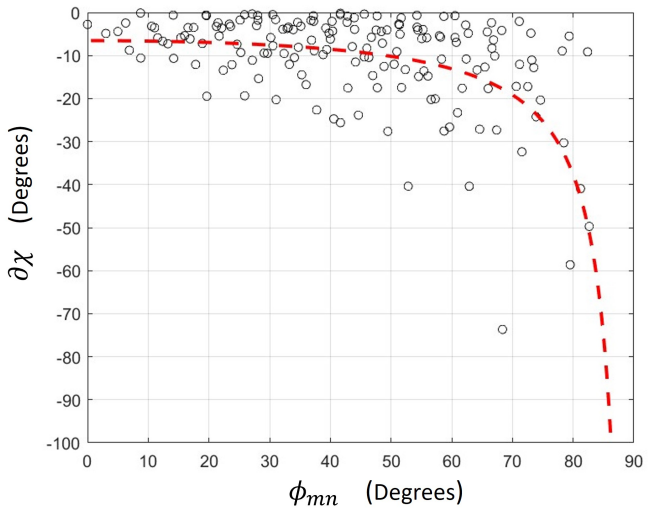

Figure 10 Change in phase $\delta\chi$ between successive modes with adjacent nil-shielding directions ϕ_{mn} for $z_0/a = 1$ and $ka = 35$.

A general trend is observed in which the phase difference between successive modes increases with increasing nil-shielding direction, although significant oscillations in the variation of χ with ϕ can be observed in figure 10. This oscillatory behaviour originates from the uneven and oscillatory values of $\delta\phi_{mn}$ between successive modes. This phase difference can be observed to be $\delta\chi \lesssim 20°$ for nil-shielding directions with angles below $\phi_{mn} < 70°$, which corresponding roughly to the range of radiation angles at which good agreement between the free-field and ducted solutions are observed in figure 6c. At high radiation angles, the phase difference between successive modes begins to increase, leading to significant oscillations in the far-field directivity caused by destructive interference between the modes arriving at the duct open end.

The phase differences plotted in figure 10 above have been demonstrated to be the cause of oscillations in the directivities shown in figures 6 when the source is deep within the duct. A simple analysis is now performed to quantify this phase difference between successive modes propagating along the duct.

An expression is now derived for the *average* phase difference $\overline{\delta\phi}$ between successive modes at any frequency ka with mean nil-shielding direction ϕ. Note that in this analysis, modes with negative m value (phase fronts spinning counter-clockwise) have been omitted since these have identical nil-shielding direction to the corresponding mode with positive m value. Modes with azimuthal order m or $-m$ with the same radial order n arrive at the duct open end perfectly in phase. The number of modes $\delta N(ka, \phi)$ with nil-shielding directions per unit range of

angles $\delta\phi$ is given by,

$$dN(ka,\phi)/d\phi = N(ka)n(\phi), \tag{21}$$

where $N(ka)$ is the total number of propagating modes with $m \geq 0$ at frequency ka and $n(\phi)$ is the modal density function, which specifies the relative number of modes with nil-shielding directions in a unit range of angles $\delta\phi = 1$, which has the normalisation property $\int_0^{\frac{\pi}{2}} \backslash(\phi)d\phi = 1$. Following Rice [19] $N(ka) \approx (1/2ka)^2$ and $n(\phi) = \sin 2\phi$. The latter has been derived from the modal density function derived by Rice in terms of cut-off ratio and making a change of variable indicated in Eq. 9 between cut-off ratio κ_{mn}/k and modal propagation angle ϕ. The average difference between successive nil-shielding directions $\overline{\delta\phi}$ is therefore given by $\overline{\delta\phi} = (dN(ka,\phi)/d\phi)^{-1}$. Substituting this expression into Eq. 20 and substituting for $n(ka)$ and $\mathit{N}(\phi)$ gives the following expression for the average difference in phase accumulated by successive modes in propagating unit length along the duct of the form,

$$\delta\chi = \frac{-k}{(\frac{1}{2}ka)^2\cos\phi}\,. \tag{22}$$

This equation is plotted in red in figure 10, which can be observed to provide a general fit to the trend in the exact variation of phase difference between successive modes, with greatest phase difference being predicted for near cut-off modes.

V Sound power radiation by free-field and ducted sources

In the previous sections, the difference in the directivities between a rotating point dipole source in a free-field and within a hard-walled, semi-infinite, circular duct is investigated. This has shown that the level of agreement between the two solutions is mostly determined by the number and density of nil-shielding directions at which the solutions are identical. In this section, the acoustic power $W(\omega)$ radiated by the free-field and ducted sources is investigated to assess the global effect on far-field radiation owing to the introduction of a duct.

The radiated sound power is calculated by integrating the far-field sound intensity,

$$W(\omega) = \frac{2\pi}{\rho_0 c_0} R^2 \int_0^{\pi} \overline{p^2}(R,\phi,\omega)\sin\phi d\phi\,, \tag{23}$$

where $\overline{p^2}(R,\phi,\omega)$ is the far-field mean square pressure due to either the free-field or ducted far-field pressure solutions of Eq. 16 or 14 respectively. The sound power from a free-field rotating point dipole source can be

deduced analytically by the substitution of Eq. 16 into 23, which gives,

$$W^{(ff)}(\omega) = \frac{1}{12\pi} k^2 \frac{\overline{F^2}}{\rho_0 c_0}, \tag{24}$$

where a 'flat' frequency spectrum for $F(\omega)$ has been assumed, as in Section III.

.

V.A Effect of sound power due to source axial distance from the open end

In this section the effect of the source's distance from the duct open end on the radiated sound power is investigated. Figure 11 shows a plot of the free-field and ducted sound powers versus ka for $z_0/\lambda = 5$ and $z_0/\lambda = 0.01$ for $r_0/a = 0.5$ and $\gamma = 0°$. Also shown is the free-field sound computed from Eq. 24, where a duct radius of $a = 1$ has been assumed to compute the frequency k since the free-field sound power radiation is independent of source radius r_0.

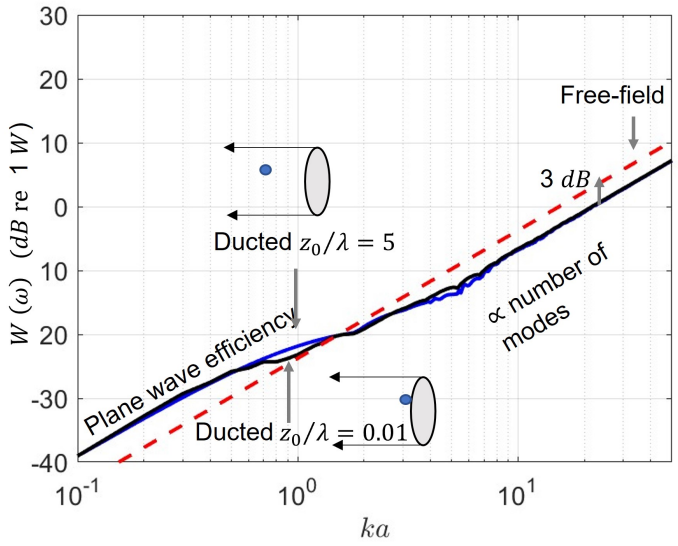

Figure 11 Power radiated by free-field and ducted sources for $r_0/a = 0.5$, $\gamma = 0°$ at $z_0/\lambda = 5$ (solid black line) and $z_0/\lambda = 0.01$ (solid blue line)

The free-field and ducted sound powers can be observed to vary as $(ka)^2$ over most of the frequency range in figure 11. This dependence on frequency is seen explicitly in the free-field sound power expression of Eq. 24. The $(ka)^2$ frequency dependence for the ducted source has different interpretations at low and high frequencies.

At low frequency, $ka < 1.84$, the $(ka)^2$ frequency dependence of the radiation efficiency for plane waves is a well-known classical result. The radiation efficiency for un-flanged and flanged ducts is well known to approach $1/2(ka)^2$ and $(ka)^2$ respectively as $ka \to 0$, Kinsler and Frey [20].

The approximate $(ka)^2$ dependence observed in figure 11 at higher frequencies, $ka \gtrsim 5$, arises because the *relative* mode amplitude distribution is independent of ka, as demonstrated by Rice [19]. Increasing frequency, therefore, only has the effect of increasing the number of propagating modes. The variation in total sound power radiation is therefore proportional to the number of modes, which varies as $(ka)^2$.

As the frequency increases a notable frequency is reached when the free-field and ducted sound powers are equal, which in this example is approximately $ka \approx 1.5$ and therefore close to the cut-on frequency of the first higher order duct modes $(m, n) = (1, 1)$. As the frequency is increased further the free-field sound power is greater than the ducted power by power by 3 *dB*, which as seen in figure 6, is due to shielding of the rear-arc radiation by the semi-infinite duct. Finally, note there is negligible difference at almost all frequencies between the sound power radiation for when the source is at $z_0/\lambda = 5$ and when the source is at the open end $z_0/\lambda = 0.01$. In this low frequency limit, in this example the ducted source radiates greater sound power than when in free-field by approximately 4.8 *dB*, identifying the higher power radiation of the plane wave from the ducted case than the free-field dipole. The plane wave and the free-field dipole radiate with similar strength on axis, but the free-field dipole has a notable null in the sideline directions where the plane wave generally radiates equally in all directions at low frequency.

V.B Effect of sound power due to source radii of rotation

This section presents an investigation of the effect of the radius of rotation r_0 on the radiated sound powers due to free-field and ducted sources. In particular, we examine the sound power ratio $\eta(\omega)$ defined by,

$$\eta(\omega) = \frac{W^{(D)}(\omega)}{W^{(ff)}(\omega)} \, . \tag{25}$$

Noting that the expression for free-field sound power, which is independent of r_0, $W^{(ff)}(\omega)$, may be written in the analytic form of Eq. 24, the sound power ratio reduces to,

$$\eta(\omega) = \frac{12\pi\rho_0 c_0}{k^2\overline{F^2}} W^{(D)}(\omega) \, . \tag{26}$$

By way of example, the sound power ratios at the three radii of rotation, $r_0/a = 0, 0.95$, and 1 were computed. Figure 12a shows the results for an axial dipole source ($\gamma = 0$) deep within the duct, $z_0/\lambda = 5$, while Figure 12b shows results for a source near the open end $z_0/\lambda = 0.01$, as a function of frequency.

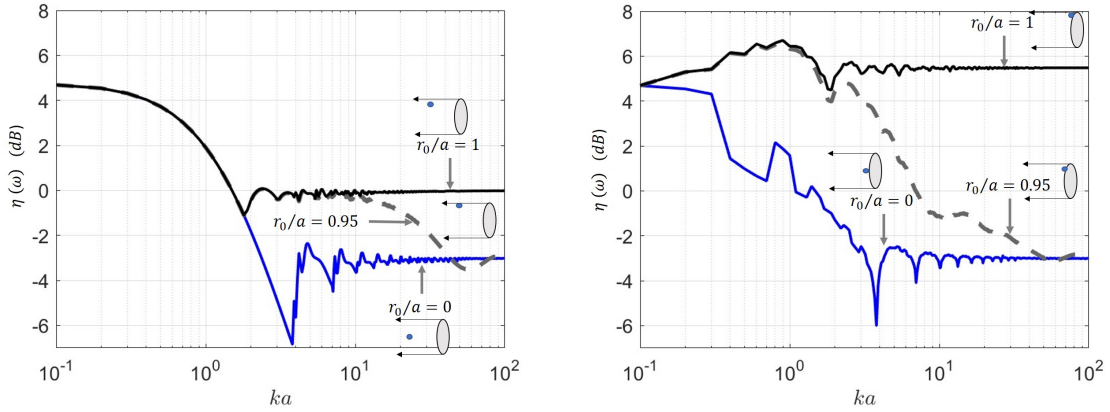

(a) $z_0/\lambda = 5$ **(b)** $z_0/\lambda = 0.01$

Figure 12 Sound power ratio of rotating point dipole sources with $\gamma = 0°$, $z_0/\lambda = 5$ and $z_0/\lambda = 0.01$ and $r_0/a = 0, 0.95$ and 1. In *dB* re 1

When the source is deep within the duct, as shown in figure 12a, identical sound power is radiated at all three radial positions below the first duct cut-off frequency $ka = 1.84$ where only the plane wave is present. For the two source radii not at the wall, $r_0/a = 0, 0.95$, $\eta(\omega) \to 1/2$. This behaviour is clearly seen in the directivity plots of figure 7 in which the ducted and free-field directivities are almost identical in the forward-arc but with zero radiation in the rear-arc due to the shielding effect by the duct. However, when the source is located on the hard duct wall, a doubling of radiated sound power occurs, but which is confined to the forward-arc such that $\eta(\omega) \to 1$ in the high frequency limit. The results at $r_0/a = 1$ and $r_0/a = 0$ appear to provide high frequency limiting values since the results at $r_0/a = 0.95$ are bounded by these two curves as $ka \to \infty$.

Different behaviour in the sound power ratio $\eta(\omega)$ is observed when the source is located close to the duct open end. Figure 12b shows that when the axial dipole source is on the rim of the duct $z_0/\lambda = 0, r_0/a = 1$, the frequency variability of $\eta(\omega)$ is much weaker and is close to 6 dB. Reference to figure 7b and 7d suggests that locating the axial dipole exactly on the duct rim fundamentally alters its radiation characteristics to that almost identical to a monopole source. As in figure 12a the sound power results at $r_0/a = 0$ and $r_0/a = 1$ appear to provide bounds on the behaviour for arbitrary source radii where now the transmission from the upper to lower curves occurs at a lower frequency when the source is located at the open end. Comparison between the curves

for the source near and at the duct wall, $r_0/a = 0.95$ and $r_0/a = 1$, identifies that the increase in ducted power radiation is only observed for sources very near the wall, as even for $r_0/a = 0.95$ frequencies above $ka \gtrsim 30$ have similar behavior to sources on the duct axis $r_0/a = 0$.

V.C Effect of sound power due to source orientation

Finally, the variation in the sound power ratio between free-field and ducted dipole sources is investigated due to varying the dipole orientation γ. Figure 13 shows the power ratio $\eta(\omega)$ of Eq. 25 for a dipole source deep within the duct $z_0/\lambda = 5$, $r_0/a = 0.5$ for the three dipole orientations $\gamma = 0°, 45°$ and $90°$. Note that the free-field sound power does not depend on dipole orientation, as shown in Eq. 24 and varies as ω^2 for constant source strength.

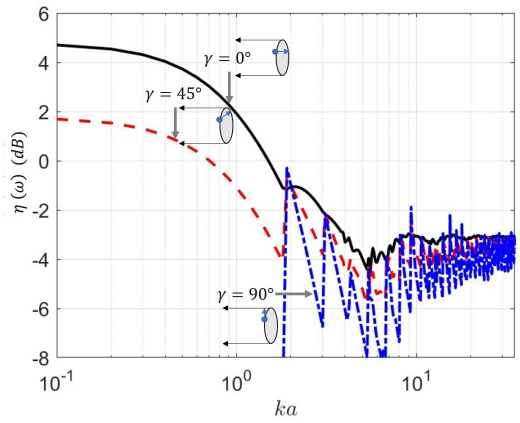

Figure 13 Sound power ratio of rotating point dipole sources with $z_0/\lambda = 5$, radius of rotation $r_0/a = 0.5$ and $\gamma = 0°, 45°$ and $90°$.

The sound power ratio in figure 13 shows a high dependence on the dipole orientation γ in the plane wave frequency range $ka < 1.84$. This behaviour is predicted by the combination of the expression for the plane wave amplitude of Eq. 54 in Appendix A and Eq. 23 for the sound power. Together these results indicate that the ducted sound power radiation varies proportional to $\cos^2\gamma$. Zero radiation is therefore produced for the transverse dipole whose dipole strength is normal to the particle velocity, leading to zero sound power radiation.

At higher frequencies, the sound power of the ducted case generally reduces with increasing dipole orientation γ and becomes more oscillatory. The reasons for both behaviours can be found in the expression for the in-duct modal amplitude of Eq. 50. As γ is increased the relative contribution from the zero azimuthal mode order $m = 0$, which makes the largest overall contribution, become comparatively weaker compared to the mode orders

$m \neq 0$, leading to weaker overall sound power radiation. Furthermore, as γ is increased the modal weightings of these non-axisymmetric modes increases, which increases the significance of the oscillations observed at the modal cut-on frequencies.

VI Conclusion

This paper presents an investigation on the characteristics of the far-field radiation from rotating point dipole sources radiating in a free-field and from a semi-infinite hard-walled circular duct. The study was motivated by the need to identify the effect on far-field radiation as a consequence of enclosing the source in a duct, as is commonly undertaken in many rotor or propeller applications to enhance their efficiency. The conclusions from this paper may be summarised as follows:

1) The concept of nil-shielding directions ϕ_{mn}, first proposed by Chapman [1], has been investigated numerically, in which the far-field directivity from a hard-walled duct is precisely equal to that in free-field at the mode-ray angles, Eq's 10 and 2.
2) For sources deep within the duct the far-field directivity tends to oscillate around the free-field result due to phase interference between different radial mode orders n of the same azimuthal mode order m (figure 6). These oscillations tend to zero as the source is introduced closer to the duct open end.
3) For sources deep within the duct, such that only propagating modes radiate significantly, the number of nil-shielding directions increases as ka (figure 3). In this high frequency limit, therefore, agreement between the free-field and ducted multi-mode solutions therefore tend to agree over all radiation angles and not just at ϕ_{mn}, except very close to the side-line directions where reflections of the near cut-off modes become significant.
4) When the source is located at the open end of the duct, but not at the duct wall, good agreement is observed even at low frequencies over all radiation angles between the free-field and ducted multi-mode solutions (figs 4, 5 and 6), signifying the importance of cut-off modes for sources located close to the open end.
5) For sources located exactly at the duct wall a doubling of the sound power occurs (figure 7).
6) For axial dipole sources located on the duct rim the far-field directivity becomes fundamentally different from that of the free-field result, and more closely resembles that of a monopole source (figure 7). However, its area-weighted average is twice that of the free-field result in the forward-arc, so that the total sound radiated from the duct is almost identical to that radiated into free-field (figure 12a) at frequencies above the first

cut-off frequency.

Acknowledgments

Funding for this work is gratefully received from the Engineering and Physical Sciences Research Council and the Defence Science and Technology Laboratory. The authors would like to express their gratitude to Gwenael Gabard for supplying the program used to compute the modal directivity factor for the un-flanged duct.

Appendices

A Derivation of free-field rotating point dipole sources

This section summarises the derivation of the expression for the frequency spectrum of the far-field acoustic pressure due to a rotating point dipole source radiating into free-field, the angular velocity of the dipole is assumed constant.

The pressure field $\hat{p}^{(ff)}(r, \theta, z, t)$ due to a rotating point source at a single axial plane $z = 0$ can be deduced from the inhomogeneous wave equation in cylindrical polar coordinates defined in figure 1 of the form,

$$\frac{\partial^2 \hat{p}^{(ff)}}{\partial r^2} + \frac{1}{r}\frac{\partial \hat{p}^{(ff)}}{\partial r} + \frac{1}{r^2}\frac{\partial^2 \hat{p}^{(ff)}}{\partial \theta^2} + \frac{\partial^2 \hat{p}^{(ff)}}{\partial z^2} - \frac{1}{c_0^2}\frac{\partial^2 \hat{p}^{(ff)}}{\partial t^2} = \hat{s}(r_0, \hat{\theta}_0, t_0)\delta(z - z_0), \tag{27}$$

where the receiver and source time are related by $t = t_0 - R/c_0$, note the observer is assumed to be in the far-field where it can be assumed $R >> z_0$. In this paper we confine our attention to a point force with arbitrary time dependence orientated at an angle γ between the azimuthal θ and axial z directions, with zero component in the radial r direction, and azimuthal θ and axial z components given by,

$$\boldsymbol{F}(t_0) = \begin{bmatrix} 0 \\ F(t_0)\sin\gamma \\ F(t_0)\cos\gamma \end{bmatrix}, \tag{28}$$

The source term $\hat{s}(r_0, \hat{\theta}_0, t_0)$ is then obtained from the divergence $\nabla \cdot \boldsymbol{F}$, of Eq. 28,

$$\hat{s}(r_0, \hat{\theta}_0, t_0) = \left[\frac{1}{r}\frac{\partial F(t_0)}{\partial \theta}\sin\gamma + \frac{\partial F(t_0)}{\partial z}\cos\gamma\right]\frac{\delta(r - r_0)}{r_0}\delta\big(\theta - \hat{\theta}_0\big), \tag{29}$$

[8], where $\hat{F}(t_0)$ is the magnitude of the fluctuating force. The solution to Eq. 27 is obtained in the wavenumber domain by first Fourier transforming the pressure with respect to z, t_0, and expanding the pressure as a Fourier series in θ, to give the following expression for the pressure due to a single azimuthal mode m,

$$\tilde{p}_m^{(ff)}(r, k_z, \omega) = \int_{-\infty}^{\infty}\int_0^{2\pi}\int_{-\infty}^{\infty}\hat{p}^{(ff)}(r, \theta, z, t)\mathrm{e}^{j(m\theta + k_z z - \omega t_0)}dz d\theta dt_0. \tag{30}$$

where k_z is the axial wavenumber, which takes continuous values in the range $-\infty$ to ∞. In the wavenumber domain the derivatives of Eq. 30 are as follows,

$$\frac{\partial}{\partial z} \rightarrow -jk_z \qquad \frac{\partial}{\partial \theta} \rightarrow -jm \qquad \frac{\partial}{\partial t} \rightarrow j\omega, \tag{31}$$

Fourier Transforming the in-homogeneous wave equation *Eq. 27* as in *Eq. 30* leads to,

$$\begin{aligned}\frac{\partial^2 \tilde{p}_m^{(ff)}}{\partial r^2} + \frac{1}{r}\frac{\partial \tilde{p}_m^{(ff)}}{\partial r} + \left(\kappa^2 - \frac{m^2}{r^2}\right)\tilde{p}_m^{(ff)} = -j\frac{\delta(r - r_0)}{r}\int_{-\infty}^{\infty}\mathrm{e}^{jk_z z}\delta(z - z_0)dz \\ \int_{-\infty}^{\infty}\int_0^{2\pi}\left(\frac{m}{r}\sin\gamma + k_z\cos\gamma\right)\hat{F}(t_0)\mathrm{e}^{j(m\theta - \omega t_0)}\delta(\theta - \hat{\theta}_0)d\theta dt_0,\end{aligned} \tag{32}$$

where κ is the radial wavenumber, which is related to the axial wavenumber k_z by the dispersion relationship $k^2 = \kappa^2 + k_z^2$. The integrals across z and θ in *Eq. 32* are evaluated using the sifting property of the Delta function,

$$\frac{\partial^2 \tilde{p}_m^{(ff)}}{\partial r^2} + \frac{1}{r}\frac{\partial \tilde{p}_m^{(ff)}}{\partial r} + \left(\kappa^2 - \frac{m^2}{r^2}\right)\tilde{p}_m^{(ff)} = -j\mathrm{e}^{jk_z z_0}\frac{\delta(r-r_0)}{r}\left(\frac{m}{r}\sin\gamma + k_z\cos\gamma\right) \int_{-\infty}^{\infty} \hat{F}(t_0)\mathrm{e}^{j(m\theta_0 - \omega t_0)}dt_0. \tag{33}$$

It is convenient to introduce the coordinate system rotating with the dipole $\tilde{\theta}_0$, defined as,

$$\tilde{\theta}_0 = \Omega t_0 + \hat{\theta}_0, \tag{34}$$

Substituting $\tilde{\theta}_0$ of *Eq. 34* into *Eq. 32* gives,

$$\frac{\partial^2 \tilde{p}_m^{(ff)}}{\partial r^2} + \frac{1}{r}\frac{\partial \tilde{p}_m^{(ff)}}{\partial r} + \left(\kappa^2 - \frac{m^2}{r^2}\right)\tilde{p}_m^{(ff)} = -j\mathrm{e}^{j(k_z z_0 + m\tilde{\theta}_0)}\frac{\delta(r-r_0)}{r}\left(\frac{m}{r}\sin\gamma + k_z\cos\gamma\right) \int_{-\infty}^{\infty} \hat{F}(t_0)\mathrm{e}^{-j(\omega - m\Omega)t_0}dt_0. \tag{35}$$

The integral with respect to t_0 in *Eq. 36*, is the inverse Fourier transform, which is readily evaluated to give,

$$\frac{\partial^2 \tilde{p}_m^{(ff)}}{\partial r^2} + \frac{1}{r}\frac{\partial \tilde{p}_m^{(ff)}}{\partial r} + \left(\kappa^2 - \frac{m^2}{r^2}\right)\tilde{p}_m^{(ff)} = -j\mathrm{e}^{j(k_z z_0 + m\tilde{\theta}_0)}\frac{\delta(r-r_0)}{r}\left(\frac{m}{r}\sin\gamma + k_z\cos\gamma\right)F(\omega - m\Omega). \tag{36}$$

Equation 36 can be solved using the method of variation of parameters. Taking the right hand side to be equal to 0, reveals Bessel's differential equation. The solution of the inhomogenius problem is given by the method of variation of parameters following McAlpine et al [8],

$$\tilde{p}_m^{(ff)}(r,\theta,k_z,\omega) = \frac{\pi}{2}F(\omega - m\Omega) \left(H_m^{(2)}(\kappa r)\int_0^r J_m(\kappa r)\delta(r-r_0)\left(\frac{m}{r}\sin\gamma + k_z\cos\gamma\right)dr - J_m(\kappa r)\int_0^r H_m^{(2)}(\kappa r)\delta(r-r_0)\left(\frac{m}{r}\sin\gamma + k_z\cos\gamma\right)dr\right), \tag{37}$$

where $H_m^{(2)}(\kappa r)$ is the Hankel function of the second kind, $H_m^{(2)}(\kappa r) = J_m(\kappa r) - jY_m(\kappa r)$, where $Y_m(\kappa r)$ is the Bessel function of the second kind. Solving the integrals across r in Eq. 37 utilising the shifting property of the Delta function for $r > r_0$, valid in the far-field, gives,

$$\tilde{p}_m^{(ff)}(r,k_z,\omega) = \frac{\pi}{2}\left(H_m^{(2)}(\kappa r)J_m(\kappa r_0) - J_m(\kappa r)H_m^{(2)}(\kappa r_0)\right)F(\omega - m\Omega)\left(\frac{m}{r_0}\sin\gamma - k_z\cos\gamma\right). \tag{38}$$

To ensure only outward far-field propagating cylindrical waves are considered, $r \to \infty$, we must have $J_m(\kappa r) \to 0$. Applying the inverse Fourier transform in z and inverse Fourier series in θ,

$$p^{(ff)}(r,\theta,z,\omega) = \frac{1}{(2\pi)^2}\sum_{m=-\infty}^{\infty} \mathrm{e}^{-jm\theta}\int_{-\infty}^{\infty} p_m(r,k_z,\omega)\mathrm{e}^{-jk_z z}dk_z. \tag{39}$$

which when applied to Eq. 38 gives,

$$p^{(ff)}(R,\phi,\theta,\omega) = \frac{1}{8\pi}\sum_{m=-\infty}^{\infty} \mathrm{e}^{-jm(\theta-\tilde{\theta}_0)}F(\omega - m\Omega) \int_{-\infty}^{\infty}\left(\frac{m}{r_0}\sin\gamma - k_z\cos\gamma\right)J_m(\kappa r_0)H_m^{(2)}(\kappa R\sin\phi)\mathrm{e}^{-jk_z(R\cos\phi - z_0)}dk_z. \tag{40}$$

The final step in the derivation for the far-field acoustic pressure due to a rotating free-field point dipole source is the evaluation of Eq. 40 using the method of stationary phase. When applied to Eq. 40, the integral over k_z in the far-field $R >> z_0$ is approximated by its value evaluated at the wavenumber k_z of stationary phase [8], computed to be $k_z = k\cos\phi$, and has the solution,

$$p_m^{(ff)}(R,\phi,\theta,\omega) = j^{m-1}\frac{1}{4S}\frac{a}{R}\mathrm{e}^{-jk(R-z_0\cos\phi)-jm(\theta-\tilde{\theta}_0)}J_m(kr_0\sin\phi)F(\omega-m\Omega)\left(\frac{a}{r_0}m\sin\gamma+ka\cos\phi\cos\gamma\right). \tag{41}$$

B Far-field radiation from ducted rotating point dipole sources

In this section the modal weighting $A_{mn}(\omega)$ valid above and below cut-off for point rotating dipole sources is derived.

The in-homogeneous wave equation to obtain the pressure field $\hat{p}(r,\theta,z,t)$ from a rotating point dipole source at a single axial plane in cylindrical polar coordinates *inside* an infinite duct is of the form,

$$\frac{\partial^2\hat{p}}{\partial r^2}+\frac{1}{r}\frac{\partial\hat{p}}{\partial r}+\frac{1}{r^2}\frac{\partial^2\hat{p}}{\partial\theta^2}+\frac{\partial^2\hat{p}}{\partial z^2}-\frac{1}{c_0^2}\frac{\partial^2 p}{\partial t^2}=\hat{s}(r_0,\theta_0,t_0)\delta(z-z_0), \tag{42}$$

To solve Eq. 42, a Green's function approach is used, which separates the pressure into a source term and a Green's function,

$$p_{mn}(r,\theta,z,t)=\int_S\int_{-\infty}^{\infty}\hat{s}(r_0,\hat{\theta}_0)\hat{G}_{mn}(\boldsymbol{X},t|\boldsymbol{X_0},t_0)dt_0dS(r_0,\theta_0). \tag{43}$$

where $\hat{s}(r_0,\hat{\theta}_0)$ is the source term. The frequency domain Green's function $G_{mn}(\boldsymbol{X}|\boldsymbol{X_0},\omega)$ can be determined by Fourier transform,

$$\hat{G}_{mn}(\boldsymbol{X},t|\boldsymbol{X}_0,t_0)=\frac{1}{2\pi}\int_{-\infty}^{\infty}G_{mn}(\boldsymbol{X}|\boldsymbol{X_0},\omega)\mathrm{e}^{j\,\omega(t-t_0)}d\omega. \tag{44}$$

It was shown by, for example Goldstein's [21] Eq. 1.C.13, that the frequency domain Green's function for a source at a single axial plane z_0 is of the form

$$G_{mn}(\boldsymbol{X}|\boldsymbol{X_0},\omega)=\frac{j}{2S}\Psi_{mn}(r,\theta)\Psi^*_{mn}(r_0,\theta_0)\frac{\mathrm{e}^{jk_{z,mn}(z_0-z)}}{k_{z,mn}}, \tag{45}$$

where $\Psi_{mn}(r,\theta)$ is the normalised mode shape function,

$$\Psi_{mn}(r,\theta) = \frac{J_m(\kappa_{mn} r)}{\sqrt{(1-\frac{m^2}{\kappa_{mn}^2 a^2})} J_m(\kappa_{mn} a)} e^{-jm\theta}, \tag{46}$$

which exhibits the normalisation property $\int_S |\Psi_{mn}(r,\theta)|^2 dS = S$ note the radial wave numbers κ_{mn} are assumed to those of the hard-walled duct case. The general case of a point dipole, with arbitrary orientation in the $\theta - z$ plane, has term $\hat{s}(r_0,\theta_0)$ of the form of Eq. 29, which can be substituted along with the modal Green's function of Eq. 45 into the pressure of Eq. 43 to give,

$$\begin{aligned}\hat{p}_{mn}^{(D)}(r,\theta,z,t) =& \frac{j}{4\pi S}\int_S \Psi_{mn}^*(r_0,\theta_0)\frac{\delta(r_0-r_0)}{r_0}\int_{-\infty}^{\infty}\hat{F}(t_0)\delta(\theta_0-\hat{\theta}_0) \\ & \left[\frac{1}{r}\frac{\partial}{\partial\theta}\sin\gamma + \frac{\partial}{\partial z}\cos\gamma\right]\cdot\Psi_{mn}(r,\theta)\int_{-\infty}^{\infty}\frac{\mathrm{e}^{jk_{z,mn}(z_0-z)}}{k_{z,mn}}\mathrm{e}^{j\omega(t-t_0)}d\omega dt_0 dS.\end{aligned} \tag{47}$$

Computing the integral across the surface area S in Eq. 47 utilizing the sifting property of the Delta function,

$$\begin{aligned}\hat{p}_{mn}^{(D)}(r,\theta,z,t) = \frac{j}{4\pi S}\Psi_{mn}(r,\theta)\int_{-\infty}^{\infty}\left[\frac{1}{r}\frac{\partial}{\partial\theta}\sin\gamma + \frac{\partial}{\partial z}\cos\gamma\right]\cdot\hat{F}(t_0) \\ \Psi_{mn}^*(r_0,\hat{\theta}_0)\int_{-\infty}^{\infty}\frac{\mathrm{e}^{jk_{z,mn}(z_0-z)}}{k_{z,mn}}\mathrm{e}^{j\omega(t-t_0)}d\omega dt_0.\end{aligned} \tag{48}$$

The differentiation $\partial/\partial\theta$ and $\partial/\partial z$ in Eq. 48 is computed using integration by parts,

$$\hat{p}_{mn}^{(D)}(r,\theta,z,t) = \frac{1}{4\pi S}\Psi_{mn}(r,\theta)\int_{-\infty}^{\infty}\frac{\mathrm{e}^{jk_{z,mn}(z_0-z)}}{k_{z,mn}}\left(\frac{m}{r_0}\sin\gamma + k_{z,mn}\cos\gamma\right)\int_{-\infty}^{\infty}\hat{F}(t_0)\Psi_{mn}^*(r_0,\hat{\theta}_0)\mathrm{e}^{j\omega(t-t_0)}dt_0 d\omega, \tag{49}$$

The azimuthal coordinate rotating with the dipole $\tilde{\theta}_0$ from Eq. 34 is introduced, performing this substitution into Eq. 50, noting $\Psi_{mn}^*(r_0,\theta_0)$ has azimuthal dependence $\mathrm{e}^{jm\theta_0}$, as can be seen from Eq. 46, gives,

$$\hat{p}_{mn}^{(D)}(r,\theta,z,t) = \frac{1}{4\pi S}\Psi_{mn}(r,\theta)\Psi_{mn}^{*}(r_0,\tilde{\theta}_0)\int_{-\infty}^{\infty}\frac{\mathrm{e}^{jk_{z,mn}(z_0-z)}}{k_{z,mn}}\left(\frac{m}{r_0}\sin\gamma + k_{z,mn}\cos\gamma\right)\mathrm{e}^{j\omega t}\int_{-\infty}^{\infty}\hat{F}(t_0)\mathrm{e}^{-j(\omega-m\Omega)t_0}dt_0 d\omega, \tag{50}$$

The integral across t_0 in Eq. 50 is the inverse Fourier transform in $(\omega - m\Omega)$ and is readily evaluated to give,

$$\hat{p}_{mn}^{(D)}(r,\theta,z,t) = \frac{1}{4\pi S}\Psi_{mn}(r,\theta)\Psi_{mn}^{*}(r_0,\tilde{\theta}_0)\int_{-\infty}^{\infty}\frac{\mathrm{e}^{jk_{z,mn}(z_0-z)}}{k_{z,mn}}\left(\frac{m}{r_0}\sin\gamma + k_{z,mn}\cos\gamma\right)\mathrm{e}^{j\omega t}F(\omega - m\Omega)d\omega. \tag{51}$$

Equation 51 is the Fourier transform of the frequency domain pressure, which can be extracted to show,

$$p_{mn}^{(D)}(r,\theta,z,\omega) = \frac{1}{2S}\Psi_{mn}(r,\theta)\Psi_{mn}^{*}(r_0,\tilde{\theta}_0)\frac{\mathrm{e}^{jk_{z,mn}(z_0-z)}}{k_{z,mn}}\left(\frac{m}{r_0}\sin\gamma + k_{z,mn}\cos\gamma\right)F(\omega - m\Omega). \tag{52}$$

Finally, following the classical solution for the pressure inside an infinite duct,

$$p_{mn}^{(D)}(r,\theta,z,\omega) = A_{mn}(\omega)\Psi_{mn}(r,\theta)\mathrm{e}^{-jk_{z,mn}z}, \tag{53}$$

derived by for example Goldstein [21], the modal weighting $A_{mn}(\omega - m\Omega)$ may be obtained by comparison of Eq. 52 to Eq 53, which yeilds,

$$A_{mn}(\omega - m\Omega) = \frac{1}{2S}\Psi_{mn}^{*}(r_0,\tilde{\theta}_0)\frac{\mathrm{e}^{jk_{z,mn}z_0}}{k_{z,mn}a}\left(\frac{a}{r_0}m\sin\gamma + k_{z,mn}a\cos\gamma\right)F(\omega - m\Omega) \tag{54}$$

The modal weighting $A_{mn}(\omega - m\Omega)$ can be used to predict radiation from a hard-walled duct in the far-field using,

$$p^{(D)}(R,\phi,\theta,\omega) = \sum_{m=-\infty}^{\infty}\sum_{n=1}^{\infty}p_{mn}^{(D)}(R,\phi,\theta,\omega), \tag{55}$$

where each mode radiates of the form,

$$p_{mn}^{(D)}(R,\phi,\theta,\omega) = \left(\frac{a}{R}\right) A_{mn}(\omega - m\Omega) D_{mn}(\phi, ka)\, \mathrm{e}^{-j(kR+m\theta)}, \tag{56}$$

Note the effect of reflections due to the mode reaching the open end of the duct is included in the directivity factor.

VII Bibliography

[1] Chapman, C., "Sound radiation from a cylindrical duct. Part 2. Source modelling, nil-shielding directions, and the open-to-ducted transfer function," *Journal of Fluid Mechanics*, Vol. 313, 1996, pp. 367–380,DOI:10.1017/S0022112094003113.

[2] Garrick, I., and Watkins, C. E., "A theoretical study of the effect of forward speed on the free-space sound-pressure field around propellers," Tech. rep., NASA, 1953.

[3] Hanson, D., "Compressible helicoidal surface theory for propeller aerodynamics and noise," *AIAA Journal*, Vol. 21, No. 6, 1983, pp. 881–889, https://doi.org/10.2514/3.60132.

[4] Parry, A., and Crighton, D., "Asymptotic theory of propeller noise. I-Subsonic single-rotation propeller," *AIAA journal*, Vol. 27, 1989, pp. 1184–1190, https://doi.org/10.2514/3.10838.

[5] Schulten, J., "Frequency-domain method for the computation of propeller acoustics," *AIAA journal*, Vol. 26, No. 9, 1988, pp. 1027–1035, https://doi.org/10.2514/3.10008.

[6] Peake, N., and Crighton, D., "An asymptotic theory of near-field propeller acoustics," *Journal of Fluid Mechanics*, Vol. 232, 1991, pp. 285–301, DOI:10.1017/S0022112091003695.

[7] Mao Y, Q. D., Gu Y, and Tang, H., "An exact frequency-domain solution of the sound radiated from the rotating dipole point source," *The Journal of the Acoustical Society of America*, Vol. 132, No. 3, 2012, pp. 1294–1302, doi: 10.1121/1.4742972.

[8] McAlpine, A., and Kingan, M., "Far-field sound radiation due to an installed open rotor," *International Journal of Aeroacoustics*, Vol. 11, No. 2, 2012, pp. 213–245.

[9] Blake, W. K., *Mechanics of flow-induced sound and vibration, Volume 2: Complex flow-structure interactions*, Academic press, 2017.

[10] Tyler, J., and Sofrin, T., "Axial flow compressor noise studies," Tech. rep., SAE, 1962, https://doi.org/10.4271/620532.

[11] Homicz, G., and Lordi, J., "A note on the radiative directivity patterns of duct acoustic modes," *Journal of Sound and Vibration*, Vol. 41, No. 3, 1975, pp. 283–290, https://doi.org/10.1016/S0022–460X(75)80175–1.

[12] Gabard, G., and Astley, R., "Theoretical model for sound radiation from annular jet pipes: far-and near-field solutions," *Journal of Fluid Mechanics*, Vol. 549, 2006, doi:10.1017/S0022112005008037, pp. 315–341.

[13] Myers, M., and Lan, J., "Sound radiation from ducted rotating sources in uniform motion," *1993* $15^{th} AIAA Aeroacoustics Conference$, 1993, $pp.1 - -13$.

[14] Baddour, B., Joseph, P., McAlpine, A., and Leung, R., "Significance of cut-off modes in acoustic radiation from ducts," *AIAA AVIATION 2021 FORUM*, Vol. 541, 2021, DOI:10.2514/6.2021-2299, p. 2299.

[15] Rienstra, S. W., and Tester, B. J., "An analytic Green's function for a lined circular duct containing uniform mean flow," *Journal of Sound and Vibration*, Vol. 317, No. 3-5, 2008, pp. 994–1016.

[16] Baddour, B., Joseph, P., McAlpine, A., and Leung, R., "Acoustic radiation characteristics of cutoff modes from ducts," *Journal of Sound and Vibration*, Vol. 541, 2022, p. 117306.

[17] Castres, F. O., and Joseph, P. F., "Experimental investigation of an inversion technique for the determination of broadband duct mode amplitudes by the use of near-field sensor arrays," *The Journal of the Acoustical Society of America*, Vol. 122, No. 2, 2007, doi: 10.1121/1.2747166, pp. 848–859.

[18] Ffowcs Williams, J., and Hawkings, D. L., "Sound generation by turbulence and surfaces in arbitrary motion," *Philosophical Transactions for the Royal Society of London. Series A, Mathematical and Physical Sciences*, 1969, pp. 321–342.

[19] Rice, E., and Prydz, A., "Multimodal far-field acoustic radiation pattern using mode cutoff ratio," *AIAA Journal*, Vol. 16, No. 9, 1978, https://doi.org/10.2514/3.60984, pp. 906–911.

[20] Kinsler, L. E., Frey, A. R., Coppens, A. B., and Sanders, J. V., *Fundamentals of acoustics*, John wiley & sons, 2000.

[21] Goldstein, M., *Aeroacoustics*, Lewis Research Center, 1976, pg 60 - 64.